SECED 2015 Conference: Earthquake Risk and Engineering towards a Resilient World
9-10 July 2015, Cambridge UK

SEISMIC RESPONSE AND DESIGN OF RECTANGULAR TUNNELS

Grigorios TSINIDIS[1], Kyriazis PITILAKIS[2], Christos ANAGNOSTOPOULOS[3] and Gopal MADABHUSHI[4]

Abstract: The paper presents a series of dynamic centrifuge tests that were carried out at the geotechnical centrifuge facility of the University of Cambridge, on a rectangular model tunnel embedded in dry sand. The tests are simulated by means of finite-element analysis of the coupled soil-tunnel system and the numerical results are compared and validated with the experimental data. Additional numerical analyses are carried out to examine the effects of crucial parameters on the tunnel response, such as soil-to-tunnel relative flexibility and soil-structure interface characteristics. The calibrated numerical models are then used to validate the accuracy of simplified design methods. The interpretation of both the experimental and numerical data reveals, among others, a rocking deformation mode of tunnels during seismic shaking coupled with the racking distortion and a significant effect of the soil-tunnel interface properties and soil yielding response on the amplitudes and distribution of the seismic earth pressures, the dynamic soil shear stresses as well as the dynamic internal forces of the tunnel lining. Simplified design methods, under certain conditions and assumptions, may provide reasonable and comparable results to the full dynamic analysis.

Introduction

Although recent earthquake events have demonstrated that underground structures and tunnels may undergo extensive deformations or even collapse, their seismic response has been little explored compared to the above ground structures. The lack of knowledge is more important for embedded structures of rectangular cross section, where strong soil-structure interaction effects may be mobilized in case of strong earthquakes. Several crucial issues related to the seismic response of these structures are still under investigation, including the seismic earth pressures on the side walls, the seismic shear stresses around the perimeter of the structure and the complex deformation modes during shaking. In this regard, design specifications in current seismic codes are based primarily on simplified methods, the implementation of which may lead to a substantially different seismic design for underground structures (Pitilakis and Tsinidis, 2014).

Along these lines, as series of dynamic centrifuge tests was performed on a flexible rectangular model tunnel embedded in dry sand. The tests were carried out at the "Turner beam centrifuge" of the University of Cambridge, within the TUNNELSEIS TA action of the SERIES research project (http://www.series.upatras.gr/TUNNELSEIS).

Within a second stage of the study, the test cases were modelled by means of a full dynamic analysis of the coupled soil-tunnel system. Additional numerical analyses were performed, in order to investigate the effects of salient parameters, such as the tunnel stiffness and soil-tunnel interface properties. Validated numerical models were finally employed to assess simplified methods used in tunnelling design practice.

Dynamic centrifuge testing

The centrifuge tests were performed under a centrifugal acceleration of 50 g. The models were constructed within a large Equivalent Shear Beam (ESB) container, while a specially

[1] Civil Engineer, MSc, PhD Candidate, Aristotle University, Thessaloniki, gtsinidi@civil.auth.gr
[2] Professor, Aristotle University, Thessaloniki, kpitilak@civil.auth.gr
[3] Professor, Aristotle University, Thessaloniki, anag@civil.auth.gr
[4] Professor, University of Cambridge, Cambridge, mspg1@cam.ac.uk

designed Stored Angular Momentum actuator was used to apply the earthquake input motions at the model base. The actuator is capable of applying sinusoidal or sine-sweep inputs (Madabhushi et al. 1998).

Soil deposits were made of dry Hostun HN31 sand (Table 1) reconstituted at two different relative densities of 50 % and 90 %. An automatic system was employed to form the soil deposit within the ESB container in a piecewise manner.

Table 1. Sand mechanical properties

ρ_s (g/cm^3)	e_{max}	e_{min}	d_{10} (mm)	d_{50} (mm)	d_{60} (mm)	φ_{crit} (^{o})
2.65	1.01	0.555	0.209	0.335	0.365	33

A 100 × 100 × 210 (mm) square model tunnel was manufactured by an extruded section of 6063A aluminum alloy (Table 2) having a thickness of 2 mm (Figure 1a). The selection of such a reduced lining thickness was made in order to study the effect of tunnel flexibility at an extreme end of possible real structure flexibilities. To study the effect of the soil-tunnel interface characteristics on the tunnel response, friction Hostun sand was stuck to the external face of the model-tunnel, creating a rough surface for the final test (Test 2). Figure 1b presents a typical model layout and the instrumentation scheme.

Table 2. Model tunnel mechanical properties

Unit weight, γ (kN/M^3)	Elastic modulus, E (GPa)	Poisson ratio, ν	Tensile strength, f_{bk} (MPa)
2.70	69.5	0.33	220

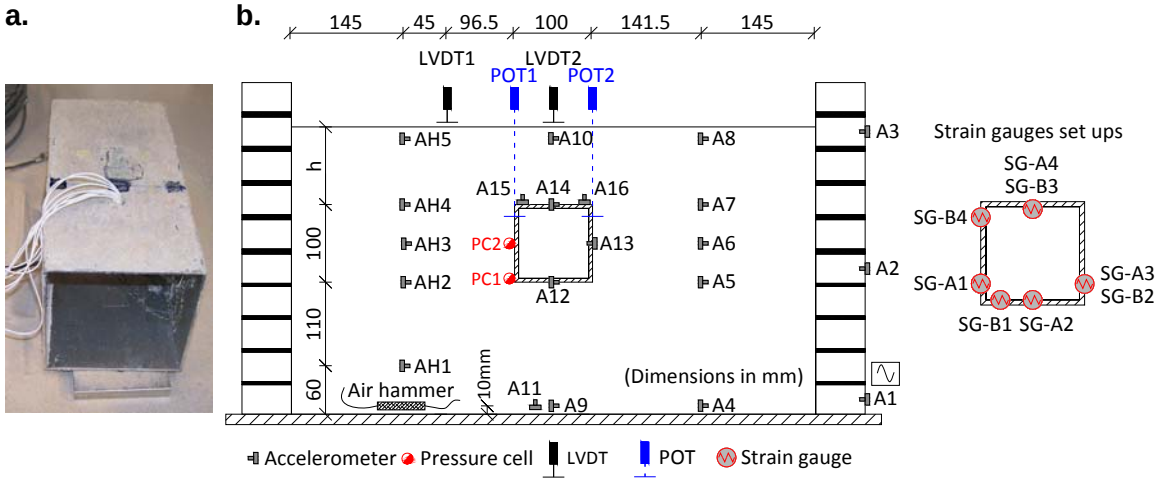

Figure 1. (a) Model tunnel, (b) typical model layout; h = 60 mm for Test 1; h = 100 mm for Test 2

A dense monitoring array was implemented to record the soil-tunnel system response, comprising of miniature accelerometers (As), linear variable differential transformers (LVDTs), position sensors (POTs) and miniature total earth pressure cells (PCs) (Figure 1b). Resistance strain gauges were also used to measure the tunnel lining axial and bending moment strains at several locations. Unfortunately, the strain gauges did not record during the first test (Test 1) due to a wiring problem, while they worked properly during the second test (Test 2). To estimate the soil shear wave velocity gradient, air hammer tests were performed prior shaking.

In each test, the centrifuge was spun up in steps until 50 g and then the earthquakes were fired in a row, leaving some time between them to acquire the data. Table 3 tabulates the sequence and characteristics of the input motions during each test. The data was recorded at a sampling frequency of 4 Hz during the centrifuge swing up and at 4 kHz during shaking. More details about the experimental program may be found in Tsinidis et al. (2014).

Table 3. Input motions characteristics (bracketed values in prototype scale)

Test ID	D_r (%)	Flight	EQ ID	Frequency (Hz)	Amplitude (g)	Nominal duration (s)
Test 1	51	1	EQ1	60 (1.2)	10.5 (0.21)	0.4 (20)
			EQ2	60 (1.2)	12.9 (0.26)	0.4 (20)
			EQ3	60 (1.2)	15.7 (0.31)	0.4 (20)
			EQ4	60 (1.2)	18.3 (0.37)	0.4 (20)
Test 2	89	1	EQ1	30 (0.6)	1.0 (0.02)	0.4 (20)
			EQ2	45 (0.9)	4.0 (0.08)	0.4 (20)
			EQ3	50 (1)	6.5 (0.13)	0.4 (20)
			EQ4	50 (1)	12.0 (0.24)	0.4 (20)
			EQ5*	60 (1.2)	12.0 (0.24)	3.0(150)
		2	EQ6	50 (1)	5.8 (0.116)	0.4 (20)
			EQ7	50 (1)	6.0 (0.12)	0.6 (30)
			EQ8	50 (1)	11.0 (0.22)	0.5 (25)

** sine sweep*

Numerical simulation

The tests were simulated by means of full dynamic time history analyses of the coupled soil-tunnel system using the finite element code ABAQUS (ABAQUS 2012). The analyses were performed in prototype scale under plane strain conditions. Figure 2 portrays a typical numerical model layout.

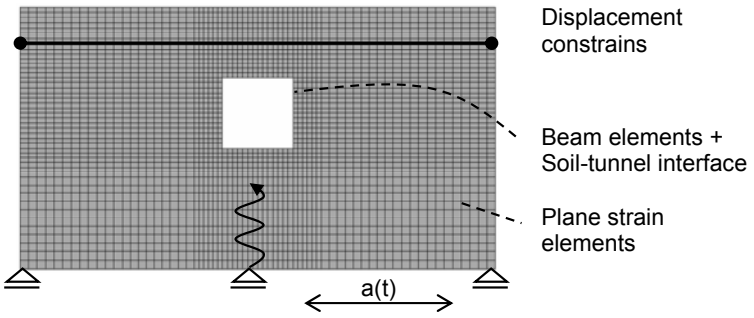

Figure 2. Typical numerical model in ABAQUS

The soil was adequately meshed with quadratic plane strain elements, while the tunnel was modelled with beam elements. The base boundary of the model was simulated as rigid bedrock, while for the vertical boundaries kinematic tie constrains were introduced, simulating in that simplified way the ESB container.

For the soil-tunnel interface, a finite sliding hard contact algorithm was implemented (ABAQUS 2012). The interface friction effect was investigated applying different Coulomb friction coefficients μ, namely μ = 0 for the full slip and 0.4 and 0.8 for slip conditions. In a final analysis, the soil and the tunnel were fully bonded assuming no slip conditions and precluding separation.

The tunnel lining behaviour was simulated using an elastic-perfectly plastic material model, with yield strength equal to 220 MPa. The dynamic sand response was modeled introducing either a visco-elastic model or a visco-elasto-plastic material with Mohr-Coulomb yield criterion, in order to account for the soil yielding response. Sand stiffness and damping were properly tuned, in order to reproduce the recorded inertial response of the soil (e.g. horizontal acceleration amplification and time histories) at free field. For this purpose, 1D soil response analyses were performed assuming a small strain shear modulus according to Hardin and Drenvich (1972) and using different sets of G-γ-D curves for cohesionless soils. Computed acceleration was compared to the recorded data. This procedure revealed that a reduced distribution according to Hardin and Drenvich (1972) was adequately describing the sand shear modulus:

$$G = a \times 100 \frac{(3-e)^2}{1+e} (\sigma')^{0.5} \quad (1)$$

where G is the shear modulus (in MPa), e is the void ratio, σ' is the mean effective stress (in MPa) and α is the reduction factor for each shake, ranging between 0.3-0.4 for the different cases studied. Viscous damping (18% for Test 1 and 15 % for Test 2) was estimated by the one-dimensional analyses and employed in the frequency depended Rayleigh type. With regard to the soil strength parameters, the friction angle φ was assumed equal to 33^o (critical angle), while the dilatancy angle ψ was assumed equal to 3^o. To avoid numerical instabilities a small amount of cohesion was introduced in the model (c = 1 kPa).

Seismic input motion was introduced at the base of the numerical model in terms of acceleration time histories referring to the motion recorded at the reference accelerometer (A1, Figure 1b). All the records were properly processed (filtering, baseline correction) before being used in the numerical analysis. Analyses were performed in two steps; first the gravity loads were introduced, while in a second step the earthquake motions were applied in a row replicating each test flight.

In a second series of analyses the lining thickness was increased to 10 mm, in order to study the effect of the tunnel rigidity on the soil-tunnel system response.

Results

This section discusses several aspects of the dynamic response of the soil-tunnel system through the presentation and comparison of relevant experimental and numerical data. The results are generally shown in model scale, if not differently stated.

Figure 3 presents representative comparisons between recorded and computed horizontal acceleration amplification along the accelerometers vertical arrays. Generally, both the visco-elastic and visco-elasto-plastic analyses reveal similar amplification. The numerical predictions are in good agreement with the records, while the differences, generally minor, are mainly attributed to the differences between the assumed soil mechanical properties (stiffness and damping) and their actual values during the test. The larger deviation of the acceleration amplitude at the tunnel roof slab in the presented example is attributed to an erroneous record at this location.

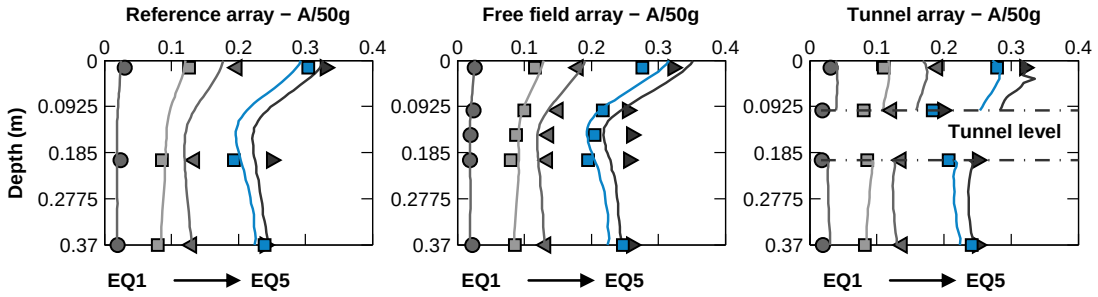

Figure 3. Horizontal acceleration amplification along the accelerometers vertical arrays for different earthquakes of Test 2 (flight 1); solid lines: numerical results from elasto-plastic analysis, markers: experimental data

Figure 4a presents representative time-windows of the recorded vertical acceleration at the sides of the tunnels roof slabs. The time histories for the deeper tunnel (Test 2) are out of phase indicating a rocking mode of vibration for the tunnel coupled with the racking distortion. Numerical results reveal a similar mode. This observation is less evident for the shallower tunnel (Test 1); however this rocking response still exists.

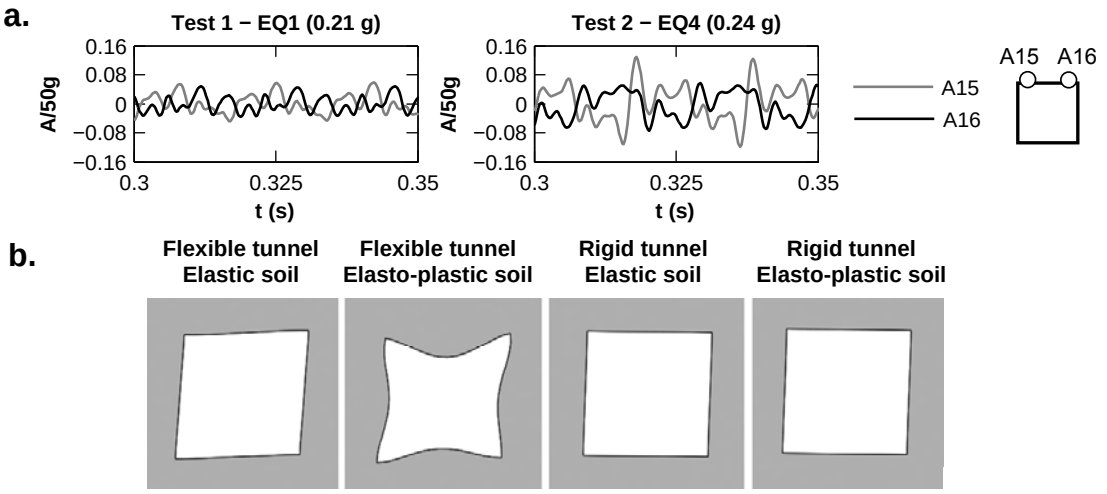

Figure 4. (a) Time windows of the recorded vertical acceleration at the sides of the tunnels roof slabs, (b) deformed shapes of deep tunnels computed for the time step of maximum racking distortion (Test 2 - EQ4, deformation scale × 60)

Figure 4b presents the computed deformed shapes of the tunnels during shaking (time step of maximum racking distortion), verifying this complex racking-rocking response. The effects of the soil yielding response and tunnel rigidity on the deformed shapes are also highlighted. Naturally, the rigid tunnel exhibits lower racking distortion than the flexible one. The increase of the tunnel flexibility results in an increase of the inward deformations of the slabs and the walls for the elasto-plastic analyses, as a result of the soil yielding response around the tunnel. As expected this effect is less evident for the rigid tunnel.

Figure 5 illustrates representative comparisons of dynamic earth pressures time histories recorded and computed at the left side-wall near the bottom corner (PC1). The effect of the soil-tunnel interface properties on the computed earth pressures is also highlighted. Residual values are observed in both experimental and numerical data resulting from the soil yielding and densification around the tunnel. This post-earthquake residual response, which is amplified with the flexibility of the tunnel, has been also reported during similar centrifuge tests (Cilingir and Madabhushi, 2011). For the deeper tunnel case (Test 2) the numerical results are closer to the experimental records for no-slip conditions, while for the shallow tunnel (Test 1) better agreement is observed for full slip conditions. It is noteworthy that for Test 2, sand was stack on the external face of the tunnel to simulate a rough interface.

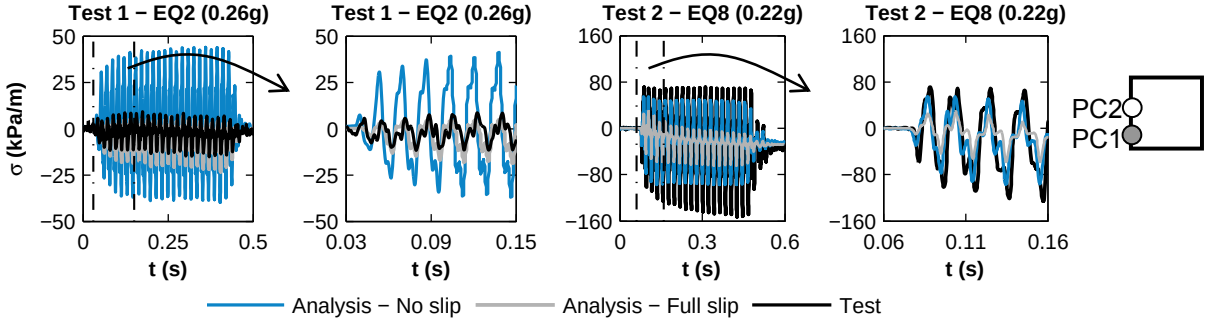

Figure 5. Dynamic earth pressure time histories recorded and computed by visco-elasto-plastic analyses near the left side-wall - invert slab corner (PC1) of the tunnels

Figure 6 illustrates the effects of the soil-tunnel interface characteristics, soil yielding response and tunnel rigidity on the dynamic earth pressure distribution computed along the perimeter of the shallow tunnel for the time step of maximum racking distortion. For elastic soil response and no-slip conditions at the interface, the results reveal an anti-symmetric

distribution of the dynamic earth pressure along the slabs and the walls. The non-linear phenomena (e.g. soil yielding and slippage at the soil-tunnel interface) result in anomalies on these distributions. The effect of the soil yielding response is more important for the flexible tunnel, due to the higher yielding response observed in this case. Full-slip condition analyses reveal larger earth pressures at the corners of the tunnel compared to the no-slip condition analyses, while the earth pressures computed for the rigid tunnel are lower than those predicted for the flexible tunnel. These observations are related to the effects of the tunnel rigidity and soil-tunnel interface properties on the stress field developed around the tunnel that affect the sand stiffness (see Equation 1). Different soil-tunnel interface properties may result in a different soil yielding response around the tunnel, thus affecting the dynamic earth pressure distributions. Similar observations are made for the deeper tunnel.

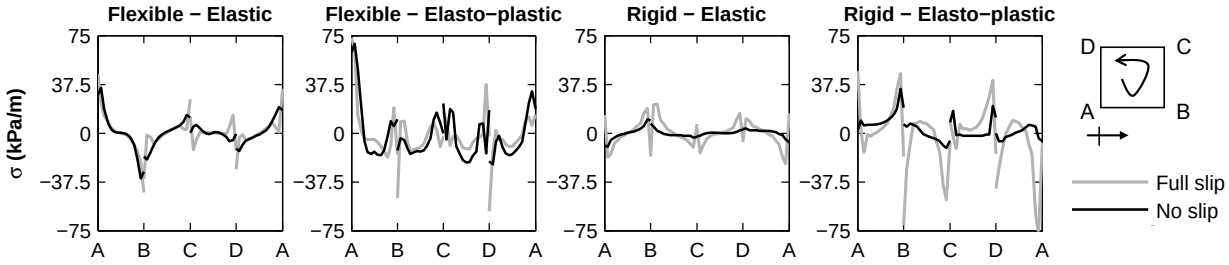

Figure 6. Effects of the soil-tunnel interface characteristics, soil yielding response and tunnel rigidity on the dynamic earth pressures distributions along the perimeter of the shallow tunnel (Test 1, EQ1)

Soil dynamic shear stresses around the tunnel are increased with the increase of the tunnel burial depth and sand relative density, while interface friction plays an important role on the shear stress distribution and magnitude. Figure 7 portrays typical soil dynamic shear stress distributions around the perimeter of the deep tunnel, computed for the time step of maximum racking distortion and for different assumptions regarding the soil-tunnel interface characteristics, soil non-linear response and tunnel rigidity. The results are compared with the soil dynamic shear stresses computed at the soil free-field at the same depth with the tunnel. Under full-slip conditions the dynamic soil shear stress distributions become sharper at the tunnel corners, while soil shear stresses are decreased at the middle sections of the slabs and walls. An increase of the soil-tunnel interface friction results in an increase of the soil shear stresses along the middle sections. Similar to the earth pressures, the soil yielding phenomena are affecting the soil shear stress making the distributions around the tunnel more complex. Interestingly, the soil shear stresses, computed at the soil free-field at the same depth with the tunnel, are compared reasonably well with the stresses computed along the perimeter of the tunnel for the no-slip conditions. The comparisons are better for elastic soil response and for the rigid tunnel. Similar conclusions are drawn for the shallower tunnel.

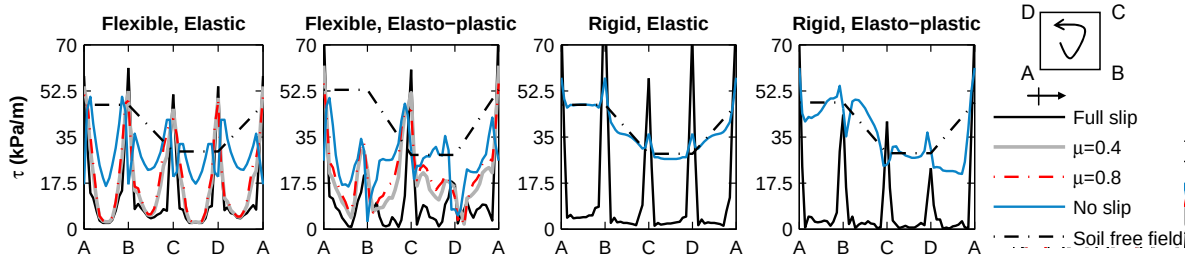

Figure 7. Effects of the soil-tunnel interface characteristics, soil yielding response and tunnel rigidity on the soil dynamic shear stress distributions along the perimeter of the deep tunnel (Test 2, EQ4)

Representative comparisons between recorded and computed by elasto-plastic analyses dynamic bending moment time histories are presented in Figure 8. Both the experimental data and the numerical predictions indicate a post-earthquake residual response, similar to

the dynamic earth pressures. This residual response is highly amplified with the tunnel's flexibility.

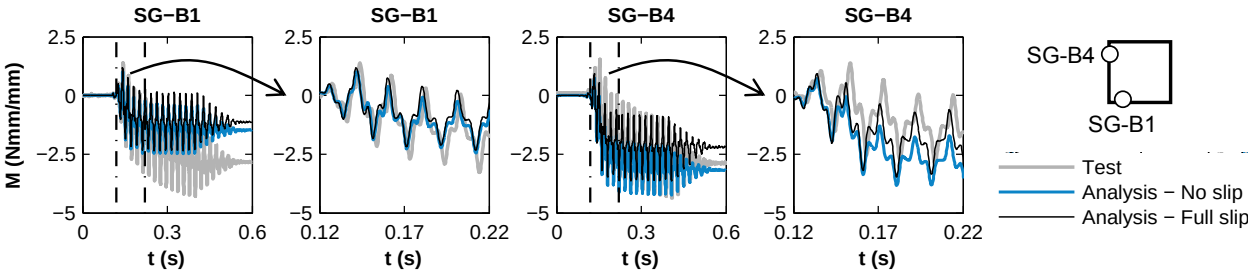

Figure 8. Dynamic bending moment time histories recorded and computed by visco-elasto-plastic analysis for Test 2, EQ3; Effect of the soil-tunnel interface characteristics

Figure 9a portrays representative distributions of the dynamic bending moment along the perimeter of the tunnel, computed by the elasto-plastic analysis for Test 2. The distributions that refer to envelope and simultaneous values (time step of maximum racking distortion) are compared reasonable well with the recorded data. Observed differences may be attributed to the discrepancies between the assumed and the actual mechanical properties of the system (sand, interface, model tunnel) and the constitutive modeling used herein. It is noteworthy that the dynamic bending moment distributions that refer to simultaneous values are quite complex and are barely following the expected anti-symmetric response along the slabs and the walls. This is a result of the increased soil yielding around the tunnel.

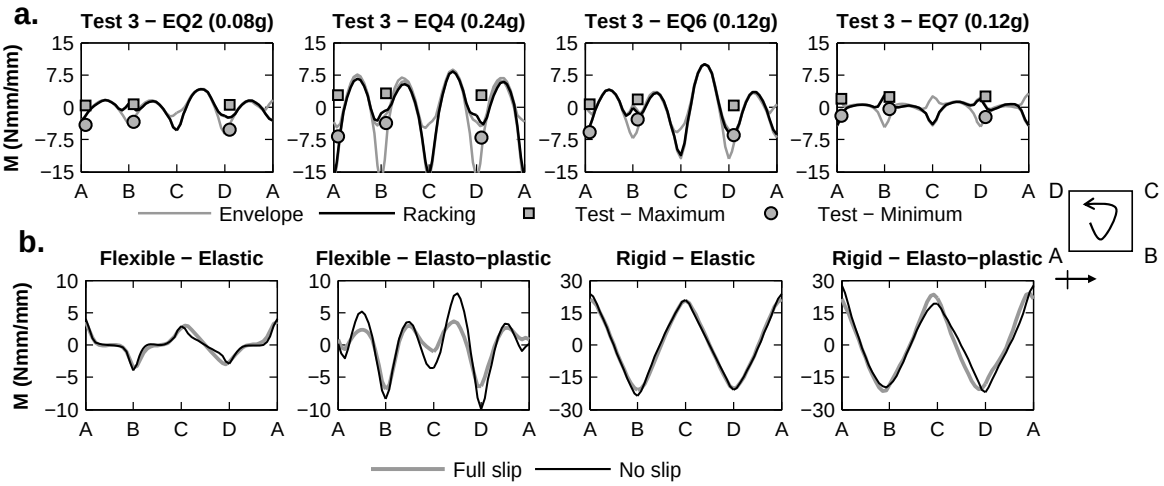

Figure 9. (a) Dynamic bending moment distributions along the perimeter of the flexible deep tunnel; Numerical predictions versus experimental data, (b) effects of the soil-tunnel interface characteristics, soil yielding behaviour and tunnel rigidity on the dynamic bending moment distributions along the perimeter of the shallow tunnel

Figure 9b illustrates the effects of the tunnel rigidity, soil yielding response and soil-tunnel interface properties on the dynamic bending moment distribution along the perimeter of the shallow tunnels. In general, the elastic analyses reveal an anti-symmetric bending moment distribution along the slabs and the walls. The non-linear phenomena (e.g. soil yielding and slippage at the soil-tunnel interface) result in anomalies on the distributions, with this effect being higher for the flexible tunnel, due to the higher yielding response around the tunnel in this case. It is noteworthy, that for the majority of the cases, the no-slip condition analyses reveal larger dynamic bending moment at the corners of the tunnel compared to the full-slip condition analyses. As mentioned before, interface properties may affect the soil yielding response around the tunnel and thus the bending moment distribution. Similar observations are made for the deeper tunnels.

Post earthquake residual values were also recorded and computed for the dynamic axial forces of the lining, resulting in complex distributions along the perimeter of the tunnels (Figure 10a). The effect of the interface characteristics is more important in this case compared to the bending moment (Figure 10b). The no-slip condition analyses reveal an anti-symmetric distribution for the dynamic axial force along the slabs and the walls, while for full-slip conditions the dynamic axial force are significantly reduced having an almost uniform distribution along the slabs and the walls. The soil yielding response may alter the axial forces distributions and magnitudes, especially in case of flexible tunnels.

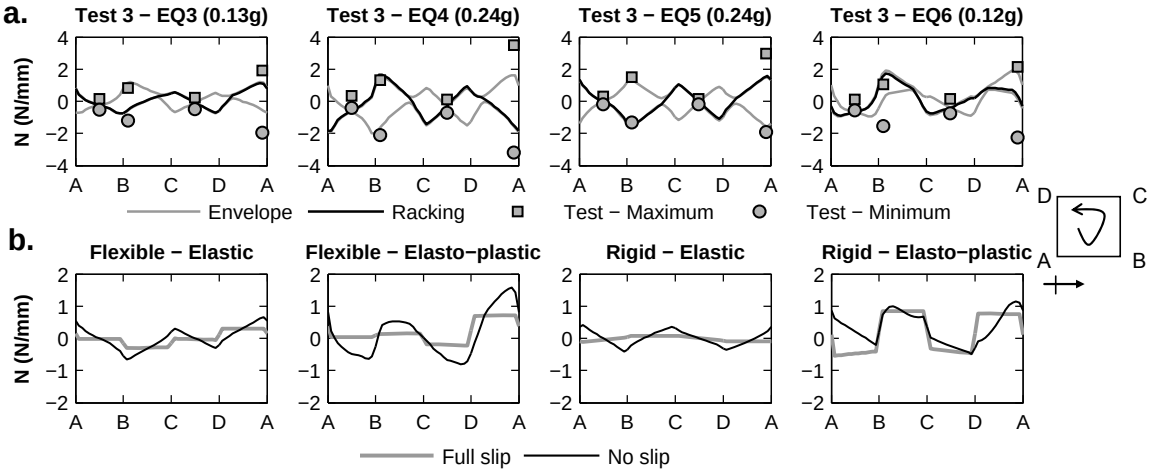

Figure 10. (a) Dynamic axial force distributions along the perimeter of the flexible deep tunnel; Numerical predictions versus experimental data, (b) effects of the soil-tunnel interface characteristics, soil yielding behaviour and tunnel rigidity on the dynamic axial force distributions along the perimeter of the shallow tunnel

Evaluation of simplified analysis methods

Test 2 was used as a case study for the validation of the detailed equivalent static analysis method (FHWA, 2009) and the simplified method proposed by Wang (1993). The analyses were performed for both the flexible model tunnel (flexibility ratio according to Wang, F= 62.5) and the rigid tunnel (F =0.29). The results of these methods were compared to the calibrated full dynamic analysis that was used as the benchmark case.

The equivalent static analyses were performed using the numerical model presented in Figure 2. The equivalent seismic load was introduced either as equivalent inertial load throughout the numerical model or as ground displacement pattern applied at the boundaries of the numerical model (Hashash et al., 2010). Both elastic and elasto-plastic analyses were performed assuming either full-slip or no-slip conditions for the interface. Sand mechanical properties (e.g. stiffness and strength) were selected in order to correspond to that of the dynamic analysis, while the equivalent seismic loads (e.g. inertia forces or ground displacements) were computed from the dynamic analysis, referring to the free field and for the time step of maximum tunnel racking distortion. To investigate the effect of the input motion amplitude, the analyses were performed for EQ3 (0.13 g) and for EQ4 (0.24 g) according to Table 3. To study the input motion frequency content on the response, a final set of analyses was performed using the JMA record from the 1995 Kobe earthquake scaled down to 0.24 g. The results presented in the ensuing refer to extreme scenarios regarding the tunnel flexibility and therefore they should be interpreted as limit cases.

Table 4 presents representative comparisons of racking ratios estimated from different approaches for EQ4, assuming elastic soil response. Generally, the numerical results for no-slip conditions resulted in larger racking ratios (12 - 35 % larger) compared to the full slip conditions. Moreover, racking ratios computed from the equivalent static analyses seem to be slightly lower (15 - 20 %) compared to the dynamic analysis results. The NCHPR611

analytical relation (Anderson et al., 2008) overestimated the racking ratio for the flexible tunnel, while for the rigid tunnel, the numerical analyses result in a ratio larger than the analytical estimation. An underestimation of the racking ratio will result in underestimation of the lining forces (e.g. implementing Wang's method). On the contrary, an overestimation of the racking ratio may lead to an overdesign that may be considered as a conservative "safe" design concept. However overdesign is not only needlessly expensive but may lead to the stiffening of the structure that may in return change the whole response pattern in a detrimental way.

Table 4. Racking ratios estimated by different methods under the assumption of elastic soil response

Racking ratio	Dynamic analysis	Equivalent static analysis - Force	Equivalent static analysis - Displacement	Anderson et al. (2008)
Flexible tunnel – full slip	1.30	1.27	1.22	1.96
Flexible tunnel – no slip	1.46	1.42	1.40	1.96
Rigid tunnel – full slip	0.50	0.47	0.40	0.45
Rigid tunnel – no slip	0.74	0.72	0.65	0.45

Figure 11 plots ratios of the bending moment computed by the static analysis to the bending moment computed by the dynamic analysis, at the left side-wall-roof slab corner for different assumptions regarding the soil-tunnel interface properties, the soil response and the input motion characteristics. Generally, equivalent static analyses underestimate the bending moment compared to the full dynamic analysis. For the elastic analyses, the differences may reach 20 to 40 %. The discrepancies are even higher for the elasto-plastic analyses (differences up to 60 %), especially for the flexible tunnel case. The differences are generally higher for the cases where the equivalent seismic load is introduced in terms of ground displacements at the model boundaries. This may be attributed to the relatively large distance between the tunnel and the numerical model boundaries, where the ground deformation is imposed. By increasing this distance it is possible that a greater amount of induced ground strain is artificially absorbed by the soil elements, thus "relieving" the structure and altering the analysis results (Pitilakis and Tsinidis, 2014). Soil-tunnel interface properties and input motion characteristics seem to have a negligible effect on the computed ratios in case of the elastic analyses, while these parameters become more important in case of the elasto-plastic analyses (especially in case of the flexible tunnel), due to their effect on the soil yielding response.

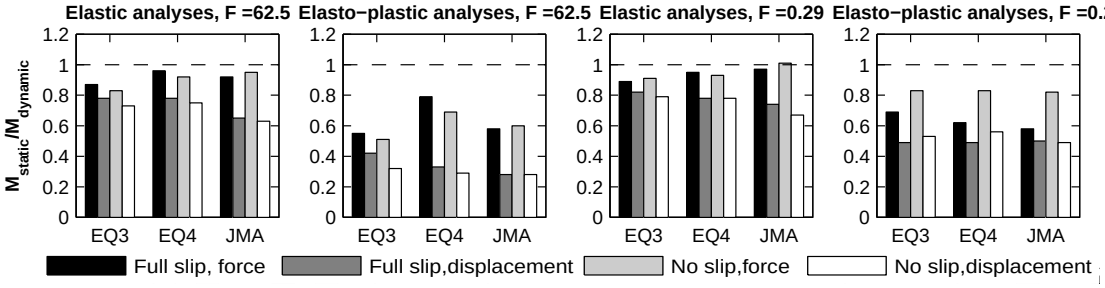

Figure 11. Bending moment computed by static analysis (M_{static}) to bending moment computed by dynamic analysis ($M_{dynamic}$) at the left side-wall - roof slab corner

Conclusions

The paper discusses several aspects of the dynamic response of rectangular tunnels in soft soils through the interpretation of representative results of dynamic centrifuge tests that were performed on rectangular model tunnels in sand as well as numerical analyses. Both the numerical and the experimental results reveal a rocking mode of vibration for the tunnel coupled with the racking distortion. Densification and soil yielding result in inward

deformations of the slabs and the walls, along with post-earthquake residual values for the dynamic earth pressures, the soil dynamic shear stresses and the lining internal forces that can not be reproduced by the elastic analyses. These response characteristics that are amplified with the tunnel's flexibility, may alter the distributions of the dynamic earth pressures, the soil dynamic shear stresses around the perimeter of the tunnel as well as the dynamic internal lining forces.

With regards to the simplified methods it has been proved that these methods should be used with caution, mainly for the preliminary stages of design, and in cases where high soil non-linearity is not expected (e.g. rather low to medium seismic intensities).

Acknoledgements
The research leading to these experimental results has received funding from the European Community's Seventh Framework Programme [FP7/2007-2013] for access to the University of Cambridge, UK under grant agreement n° 227887 [www.series.upatras.gr].

REFERENCES

ABAQUS (2012) *ABAQUS: theory and analysis user's manual version 6.12*, Dassault Systèmes SIMULIA Corp, Providence, RI

Anderson DG, Martin GR, Lam I, Wang JN (2008) *NCHPR611: Seismic analysis and design of retaining walls, buried structures, slopes and embankments*, National Cooperative Highway Research Program, Transportation Research Boards, Washington, DC

Cilingir U and Madabhushi SPG (2011) Effect of depth on the seismic response of square tunnels, *Soils and Foundations*, 51(3): 449-457

FHWA (2009) *Technical manual for design and construction of road tunnels - Civil elements, U.S. Department of transportation, Federal Highway Administration*, Publication No. FHWA-NHI-09-010, Washington DC

Hardin BO and Drnevich VP (1972) Shear modulus and damping in soils: design equations and curves. *Journal of Soil Mechanics and Foundations Division, ASCE*, 98: 667-692

Hashash YMA, Hook JJ, Schmidt B, Yao JI-C (2001) Seismic design and analysis of underground structures, *Tunnelling and Underground Space Technology*, 16(2): 247-293

Hashash YMA, Karina K, Koutsoftas D, O'Riordan N (2010) *Seismic design considerations for underground box structures*. In Proceedings of the Earth Retention Conference 3, Bellevue, WA, United states, 620-637

Madabhushi SPG, Schofield AN, Lesley S (1998) *A new stored angular momentum (SAM) based actuator*, Proceedings of the International Conference Centrifuge 98, Tokyo, Japan,111-116

Pitilakis K and Tsinidis G (2014) Performance and seismic design of underground structures, In: Maugeri M and Soccodato C (eds), *Earthquake Geotechnical Engineering Design*, Geotechnical Geological and Earthquake Engineering, 28: 279-340, Springer International Publishing, Switzerland

Tsinidis G, Heron C, Pitilakis K, Madabhushi SPG (2014) Physical modelling for the evaluation of the seismic behavior of square tunnels, In: Ilki A and Fardis M (eds.) *Seismic Evaluation and Rehabilitation of Structures*, Geotechnical Geological and Earthquake Engineering, 26: 389-406, Springer International Publishing, Switzerland

Wang JN (1993) Seismic design of tunnels: a simple state of the art design approach, Parsons Brinckerhoff, New York